)

Design and verification of a smart wing for an extreme-agility micro-air-vehicle

Viresh Wickramasinghe[1], Yong Chen[1], Marcias Martinez[1], Franklin Wong[2] and Robert Kernaghan[1]

[1] Institute for Aerospace Research, National Research Council Canada, Ottawa, ON, K1A 0R6, Canada
[2] Precision Weapons Section, Defence Research & Development Canada, Quebec City, QC, G3J 1X5, Canada

E-mail: viresh.wickramasinghe@nrc.gc.ca

Received 10 May 2011, in final form 18 September 2011
Published 23 November 2011
Online at stacks.iop.org/SMS/20/125007

Abstract
A special class of fixed-wing micro-air-vehicle (MAV) is currently being designed to fly and hover to provide range superiority as well as being able to hover through a flight maneuver known as prop-hanging to accomplish a variety of surveillance missions. The hover maneuver requires roll control of the wing through differential aileron deflection but a conventional system contributes significantly to the gross weight and complexity of a MAV. Therefore, it is advantageous to use smart structure approaches with active materials to design a lightweight, robust wing for the MAV. The proposed smart wing consists of an active trailing edge flap integrated with bimorph actuators with piezoceramic fibers. Actuation is enhanced by preloading the bimorph actuators with a compressive axial load. The preload is exerted on the actuators through a passive latex or electroactive polymer (EAP) skin that wraps around the airfoil. An EAP skin would further enhance the actuation by providing an electrostatic effect of the dielectric polymer to increase the deflection. Analytical modeling as well as finite element analysis show that the proposed concept could achieve the target bi-directional deflection of 30° in typical flight conditions. Several bimorph actuators were manufactured and an experimental setup was designed to measure the static and dynamic deflections. The experimental results validated the analytical technique and finite element models, which have been further used to predict the performance of the smart wing design for a MAV.

(Some figures may appear in colour only in the online journal)

Nomenclature

MAV	Micro-air-vehicle
EA-MAV	Extreme-agility micro-air-vehicle
MFC	Macro-fiber composite
EAP	Electroactive polymer
FEA	Finite element analysis
d_{33}	Primary piezoceramic coupling coefficient
Cp	Local pressure coefficient
ρ	Density of dry air (=1.225 kg m^{-3})
P	Pressure
V_{fs}	Free stream velocity
V_{pp}	Peak-to-peak voltage

1. Introduction

Micro-air-vehicles are small, lightweight aircraft that are being used to perform a variety of missions in an ever expanding range of operational environments. A special class of fixed-wing MAV is currently being designed to achieve the capability of hovering vertically like a rotary-wing vehicle through a flight maneuver known as prop-hanging. The fuselage of this type of extreme-agility micro-air-vehicle remains vertical during a prop-hanging maneuver because the weight of the aircraft is balanced by the thrust from the propeller. The primary requirement for this maneuver is that the thrust-to-weight ratio be greater than unity. This type of EA-MAV design provides the range superiority of a fixed-wing aircraft with the hover capabilities of a rotary-wing aircraft that are

essential for military missions such as reconnaissance and surveillance in urban environments. For example, an EA-MAV carried in a backpack could be deployed to provide situational awareness within a building by executing a hovering maneuver to gather stable reconnaissance images while, at the same time, a soldier operating the EA-MAV climbs the staircase.

The hover maneuver requires roll control of the fixed-wing aircraft through differential aileron deflections. A conventional aileron control system typically consists of a number of discrete components that contribute significantly to the gross weight and complexity of the aircraft especially in the case of a MAV. Although properly designed ailerons are effective and lightweight, these systems are relatively complex with multiple components [1]. Therefore, it is advantageous to use the smart structure approach with embedded solid state active material actuators to design a lightweight, robust and flexible wing for small unmanned aircraft. Such an aircraft would have a wing span on the order of 1000 mm with an all-up-weight under 1000 g. An example aircraft is shown in figure 1. Such a smart wing could provide sufficiently large deflection to control the MAV without traditional ailerons and facilitate folding of the wing structure for compact storage at an equivalent weight. Piezoelectric fiber actuators are highly suitable for this application due to their conformable nature, high frequency response capability and the ability to generate large actuation forces. The robustness and conformability of piezoceramic fiber based actuators have been demonstrated previously for a variety of aircraft applications [2, 3]. Furthermore, the interdigitated surface electrode pattern that makes use of the primary piezoelectric coefficient, d_{33}, increases the in-plane actuation performance [4]. For example, piezoceramic fiber actuators have been integrated into a composite helicopter blade to generate an active twist for vibration suppression [5]. In addition, piezoceramic fiber actuators have been successfully used to control the vibration of a full-scale F/A-18 aircraft vertical tail under buffet loads [6]. Although there have been several successful demonstrations, implementation in full-scale hardware has been hindered primarily due to insufficient actuation capability. The insufficient actuation capability in these applications is not only due to the limited displacement capability in piezoceramic material but also due to the fact that the actuators are used to deform an inherently stiff structure designed to satisfy strength requirements. High strength requirements are imposed on manned aircraft structures primarily due to safety concerns. In contrast, the unmanned nature of MAV enables design of flexible structures with parameters governed by performance rather than safety. This allows active material actuators to be used efficiently on MAVs with compliant wing structures by minimizing the amount of energy invested in straining the passive structures. Furthermore, the compliant wing could be designed with sufficient strength and stiffness to sustain the relatively low aerodynamic loads on an EA-MAV for reconnaissance in urban environments.

A number of approaches have been studied to improve the flight control of MAVs with active material actuators to deform a wing in lieu of traditional ailerons. It was

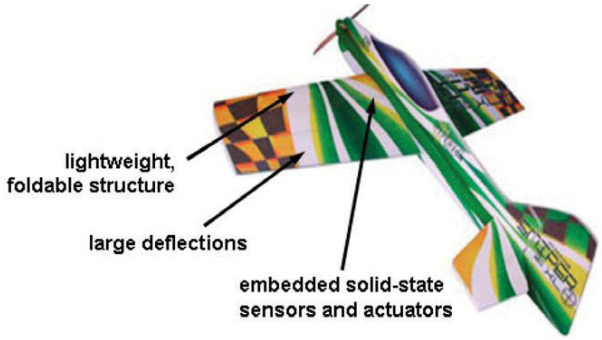

Figure 1. Conceptual extreme-agility MAV.

demonstrated that wing morphing works well for membrane wings to induce roll control on small MAVs through the use of active threads [7]. The use of piezoelectric actuators as bimorph bender actuators has produced large deformations at the trailing edge of MAVs [8]. It was also shown that the application of a preload on the actuator by means of a skin has a positive effect in achieving higher deformations up to 12° peak-to-peak deflection [9]. However, an extensive search of technical literature showed that a large airfoil shape with bi-directional deflection of approximately 30° required for EA-MAV flight control could not be achieved with a single active material actuator system.

The proposed smart wing concept for EA-MAVs consists of dual active material systems, namely the piezoceramic fiber actuators as the primary actuation mechanism and electroactive polymer as the secondary mechanism to enhance deflection performance. Integration of the two active material systems can generate a unique synergetic enhancement of the airfoil trailing edge deflection, which results from the piezoelectric effect of the bimorph actuator, compressive axial load of the pre-strained skin, and electrostatic effect of the dielectric EAP skin. This innovative active airfoil concept is expected to generate approximately 30° trailing edge deflection for effective EA-MAV flight control, but remains compact and light in weight. Analytical and FEA modeling have been performed to verify the deflection of the wing in both the wind-off and wind-on flight conditions. Wind-on surface pressures were calculated using the XFOIL aerodynamic code and applied in a loosely coupled fluid–structure analysis to estimate wing deflections. In addition, several prototype bimorph actuators were manufactured and a smart wing hardware model was assembled. An experimental setup was designed in order to measure the static and dynamic deflections. The experimental results validated the analytical and FEM models used to analyze the smart wing design for EA-MAV applications.

2. Smart wing concept

The EA-MAV smart wing design requires a controllable trailing edge deflection of approximately 30° for aerodynamic control during the prop-hanging flight maneuver. In order to achieve such a large deflection, the smart wing was designed

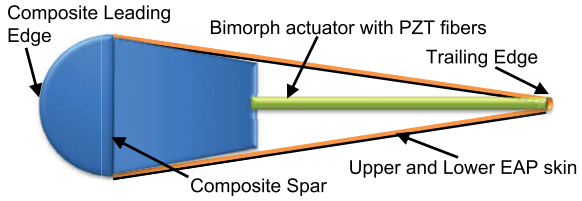

Figure 2. Cross-section of the dual actuator based smart wing design.

with an innovative dual active material combination approach to generate increased trailing edge deflections without moving mechanical components. A composite spar was used as the structure to integrate the dual actuation system and to provide the primary stiffness of the wing in the span direction. The integrated smart wing structure consisting of the composite spar, the piezoceramic bimorph actuators and the EAP based active skin is shown in figure 2 for the active trailing edge flap.

The piezoceramic fiber based bimorph actuators were used as the primary actuation mechanism of the active trailing edge flap of the smart wing. Although the piezoceramic fibers tend to crack at relatively low mechanical strains due to their inherent brittle nature, the strength and toughness properties [10] of fiber composites actuators can be significantly improved by the polymer matrix [11] that surrounds the fibers, as shown in figure 3(a). The interdigitated surface electrodes as shown in figure 3(b) can enhance in-plane actuation capability due to the use of the primary d_{33} piezoceramic coefficient. Commercially available piezoceramic fiber actuators with interdigitated electrodes, known as macro-fiber composite actuators, were used in this study [12]. A bimorph bender actuator consisting of two MFC actuators bonded on opposite sides of a thin aluminum substrate was used as the primary actuator for the active trailing edge flap. The adhesive layers not only provide the required mechanical connection between the actuator and substrate layers, but also provide the necessary electrode insulation for the two piezoelectric layers. The control voltages applied to the MFC actuators on opposing surfaces were configured to be out-of-phase in order to deflect the bimorph actuator. Several piezoceramic fiber based bimorph actuators were arranged as parallel actuators in the MAV smart wing trailing edge to obtain the continuous deflection required for active aerodynamic control.

The secondary actuation mechanism is provided by the EAP film, which is used as an active skin to enhance the actuation of the smart wing. Dielectric EAP is a special type of flexible polymer that has the ability to generate large deformation under a high electric field. Commercially available dielectric EAP material was tested for this application. This flexible dielectric film was wrapped around the composite spar, active bimorph actuators, and the trailing edge tab as shown figure 2. Application of a control voltage deformed the skin to amplify the trailing edge deflection of the active wing.

To further enhance the deflection of the piezoelectric bimorph actuators the flexible dielectric skin was pre-strained to apply an initial compressive axial load to the piezoelectric bimorph actuators. This unique integration of the MFC and EAP with preload provided a synergetic actuation enhancement to achieve a smart wing design that can produce the much larger deflection required for the EA-MAV application.

3. Smart wing model

A NACA 0009 smart wing airfoil model for the EA-MAV was designed using four bimorph actuators as the active trailing edge as seen in figure 4. The span of the prototype active wing section was approximately 300 mm. The width of the leading edge, the composite spar and the trailing edge were 65 mm, 75 mm, and 85 mm, respectively, for an overall chord of 240 mm. The center spar section of the wing was fabricated from carbon fiber pre-preg and designed to connect the active trailing edge and the leading edge of the wing. The leading edge was fabricated out of an inner foam core covered by woven carbon fiber pre-preg in order to provide the required smoothness and rigidity. Both the leading edge and the active aileron were designed for ease of detachment from the composite spar. The upper and lower skins of the wing were made out of latex or an EAP film pre-strained in tension to increase the actuation deflection of the aileron. The skin was interconnected to two tension rollers to adjust the tensional load during the initial experimental investigation. In the case of the EAP skin, control signals would be passed through a very

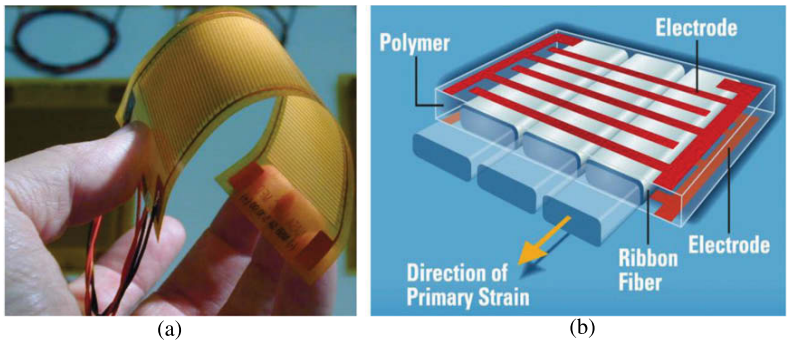

(a) (b)

Figure 3. (a) Conformable piezoceramic fiber actuators and (b) schematic of the actuator design.

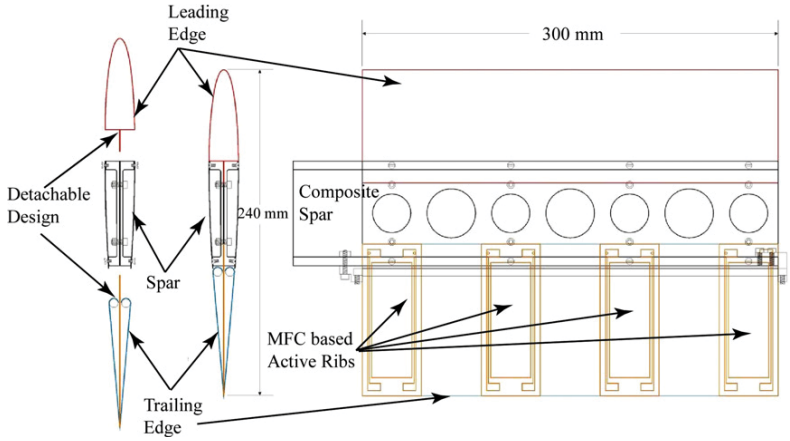

Figure 4. EA-MAV smart wing model.

Table 1. Material and geometrical properties.

	MFC actuator	PZT-5A fiber	Aluminum substrate	Epoxy polymer	Kapton insulation	EAP film
Elastic modulus (GPa)	30.0	60.9	70.0	3.4	2.05	0.035
Thickness (μm)	300	175	76	31	31	200
Density (kg m^{-3})	—	7500	2750	2750	—	—
Poisson's ratio	0.31	0.35	0.33	0.33	0.36	—
d_{33} (V m^{-1})	400×10^{-12}	374×10^{-12}	—	—	—	—

compliant electrode layer for actuation. Both analytical as well as finite element analyses have been conducted to predict the deflection performance of the smart wing model. The results are presented in the remainder of the paper.

3.1. Analytical model

Many researchers have studied the piezoelectric bimorph bender actuator concepts to predict the deflection under external control voltages [13]. An analytical model of the EA-MAV smart wing was developed to predict the deflection of the active flap consisting of bimorph actuators. The influence of multiple external loads such as the axial compression force, out-of-phase voltage application, and distributed aerodynamic load were considered in order to predict the deflection of this MAV smart wing design. It is important to note that the analytical model did not fully couple the piezoelectric and mechanical effects but they were superimposed after independent assessment of the smart wing. The analytical model consisted of a bimorph actuator that was comprised of two layers of piezoelectric actuators symmetrically bonded on either side of an aluminum substrate. It was assumed that the bonding layers as well as the substrate layers were isotropic and purely elastic. The MFC actuators were polarized in the fiber direction to generate the piezoceramic strain coefficient d_{33} and would therefore generate in-plane deformations with application of a control voltage. The model was developed based on the bending equilibrium equation of the bimorph actuator expressed as:

$$\frac{\mathrm{d}^2 z}{\mathrm{d}x^2} = \frac{M_\Lambda}{EI} + \frac{P_\mathrm{A} z}{EI} + \frac{F_Z(L-x)}{EI} + \frac{\int_0^L p_x b(L-x)\,\mathrm{d}x}{EI} \quad (1)$$

where M_Λ represents the bending moment introduced by the two MFC actuators; P_A is the axial preload; F_Z is the lumped out-of-phase force; p_x is the distributed pressure along the surface of the rib; EI is the overall bending stiffness of the bimorph actuator consisting of MFCs and the aluminum substrate. Detailed derivative equations of the analytical model have been published previously [14].

The analytical model assumed that the thickness of each layer was small compared to the radius of curvature induced by the external loads. Since the width of the bimorph actuator is much larger than the thickness, the actuator can be considered to be undergoing in-plane bending only. The model highlighted the existence of a non-linear coupling effect between the axial preload and the cantilevered flap deflection. Therefore, the deflection of the EA-MAV aileron can be effectively improved without increasing control voltage on the piezoelectric actuators by properly applying a compressive axial preload to the bimorph actuators.

The analytical model assumed typical material and geometrical properties for various components of the smart wing design, as shown in table 1. The MFC consisted of a rectangular piezoelectric PZT-5A fiber layer and an interdigitated electrode with a spacing of 0.5 mm. The manufacturer-quoted piezoceramic coupling coefficient d_{33} values shown in table 1 indicate a higher value for the MFC [15] compared to the raw PZT material [16]. In contrast, the value of the primary d_{33} for the MFC was expected to be lower than the raw PZT-5A material due to the passive material surrounding the active fiber. In order to be conservative in the performance estimates of the smart wing, the lower value of d_{33} was used for both the MFC and PZT properties in the analytical

Table 2. Predicted active rib bending deflection.

Axial preload (N)	Latex skin (deg)	Number of EAP film layers		
		1	3	5
0	13.6	14.2	15.3	16.5
15	17.0	17.7	19.2	20.7
30	21.0	22.0	23.8	25.7
40	24.2	25.3	27.5	29.8

and finite element models. The relative permittivity of EAP was 4.8. As recommended by the manufacturer, the $2000V_{pp}$ actuation voltage cycle for the MFC was −500 to +1500 V. This voltage range was used for EAP film actuation as well.

The results obtained from the analytical calculations shown in table 2 indicate an increase in tip deflection of the bimorph actuator as the compressive axial preload was increased. It is important to note that the maximum axial compressive load was limited by the buckling load of the bimorph bending actuator. The axial compressive load on the piezoelectric bimorph actuator can be achieved by properly applying a preload to the bimorph actuator either by pre-stretching the active EAP skin or a passive latex skin on the airfoil. Under an axial compressive preload of 40 N, the bimorph actuator can theoretically achieve a peak-to-peak deflection of 24.2° in contrast to 13.6° deflection without any preload.

The novelty of the proposed smart wing concept is in the use of the EAP film as an active skin over the airfoil in order to enhance the maximum deflection of the bimorph based active rib. The analytical results in table 2 show that the deflection performance increased by 4%, 13%, and 22% compared to the latex skin as the number of active EAP layers were increased from 1, 3, and 5, respectively. For an axial compressive preload of 40 N and five layers of EAP skin, the combined deflection was predicted to be as high as 29.8°. The results show that the proposed smart wing trailing edge concept could reach the deflection of 30° required for effective EA-MAV flight control.

3.2. Aerodynamic model

An analytical model was used to verify the ability of the smart wing structure to maintain the desired aerodynamic shape during maneuver of the MAV. Aerodynamic loading constitutes the primary factor that affects the performance of the smart wing actuation and the resultant deformation during flight. The actuators and stiffness of the underlying structure must be able to maintain the desired aerodynamic shape to generate the control forces that maneuver the air vehicle. Therefore, an aerodynamic model was developed to evaluate the effect of the aerodynamic loading on the smart wing design for the MAV. There are several methods to treat the coupled aero-elastic problem, which range from direct schemes involving fully coupled schemes [17] to sequential schemes [18]. As a first approximation to examine the fluid–structure interaction of the smart wing, aerodynamic loads were applied to the smart wing structure in a single step before calculating the resultant structural deformations. The aerodynamic loads were calculated according to three operational flight conditions

Table 3. EA-MAV flight conditions.

Operation	Flight speed ($m\ s^{-1}$)	Angle-of-attack (deg)	Flap deflection (deg)
Slow recon	2.8	−5 to +8	±20
Cruise	8.3	−3 to +3	±10
Dash	13.9	−2 to +2	±5

shown in table 3. These conditions covered the range of flight regimes that the smart wing is expected to experience in typical missions. Slow reconnaissance implies slow forward flight with the ability to make aggressive maneuvers if required. Dash implies fast forward flight to transit between points of interest with only small course corrections. Cruise is an intermediate condition between slow reconnaissance and dash.

The Xfoil program by Drela [19] was used to calculate the surface pressures on the airfoil with deflected surfaces. The code is capable of inviscid and viscous analyses of existing airfoils and allows predictions just beyond stall. The inviscid option was used to calculate the pressure coefficients for −5°, 0° and +5° angles-of-attack with 0° flap deflection. The viscous option was used to generate the results for flap deflections of +2°, +5°, and +20° at 0° angle-of-attack. Viscous solutions were obtained by following the procedure outlined in the Xfoil User Primer [19]. The Reynolds number, based on a 250 mm characteristic chord length, was 2.4×10^5 for 'dash' speed while the 'cruise' and 'slow recon' were 1.43×10^5 and 0.48×10^5, respectively. These values are in a flow regime where an accurate estimation of transition is needed for the calculation of representative surface pressure coefficients.

Xfoil uses the e^n method for free transition. The default N_{crit} of 9 was used for the calculations. The surface pressure, P, in engineering units was calculated according to:

$$P = (1/2)Cp\rho V_{fs}^2. \tag{2}$$

As expected, the analysis showed that the dash flight condition generated the most severe aerodynamic loads due to the high flight speed. Although not expected in a typical mission profile, the dash flight condition was analyzed with a 0° angle-of-attack and 20° flap deflection in order to generate an upper bound for the aerodynamic pressure load expected on the EA-MAV wing. The pressure difference expected over the airfoil for a typical dash flight condition with an angle-of-attack of 0° and the flap deflection of 2° is shown in figure 5. The differential pressure loading for the dash condition with an angle-of-attack of 0° and 20° of flap deflection is shown in figure 6. The pressure distribution was simplified by assuming triangular distribution with a linear reduction in pressure from flap hinge to the trailing edge tip. This triangular distribution is more conservative than the calculated pressure profile. The generated aerodynamic loads based on the simplified differential pressure profiles were then applied to the analytical model to predict the deflections under the combined piezoelectric and axial pre-compression loads. It was assumed that the resultant airfoil wing deflections did not change the aerodynamic loads significantly. Comparisons of

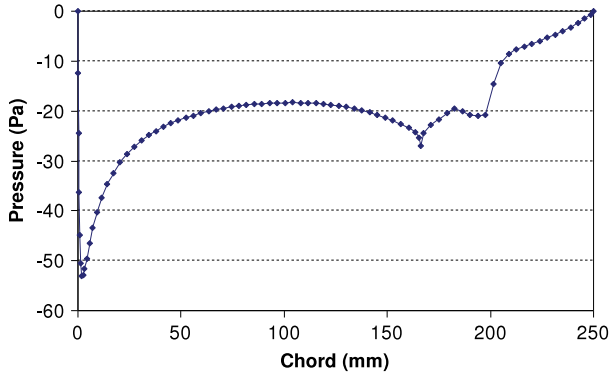

Figure 5. Differential pressure profile for dash with AOA = 0°, Flap = 2°.

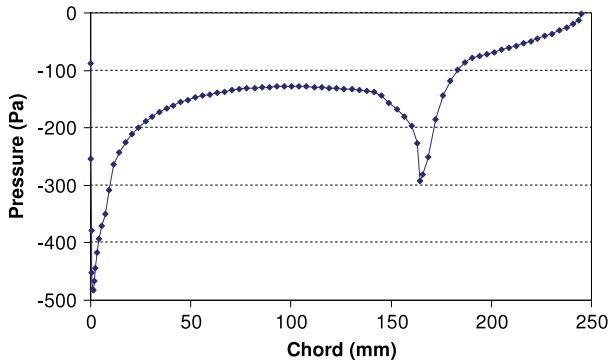

Figure 6. Differential pressure profile for dash with AOA = 0°, Flap = 20°.

the tip deflections of the active trailing edge under wind-off and wind-on conditions for dash flight with the nominal 2° flap and extreme condition at the 20° flap are listed in table 4. The results show that the loss in deflection due to aerodynamic loading is not significant for the smart wing.

3.3. Finite element model

In addition to the analytical modeling, finite element modeling was performed to gain confidence in the analytical predictions.

Table 4. Tip deflection of the active trailing edge without EAP skin.

Axial load (N)	No wind condition (deg)	Dash with 2° flap (deg)	Dash with 20° flap (deg)
0	13.6	13.5	12.8
15	17.0	16.8	16.0
35	21.0	20.9	19.7
40	24.2	24.1	22.7

The smart wing finite element modeling was performed using in-house and commercial finite element analysis (FEA) packages. An in-house finite element analysis package, based on a piezoelectric linear elastic model, was used to verify the actuation of the bimorph actuator consisting of MFCs as well as PZT wafers [20]. Details of this linear finite element model and the actuation results have been published previously [21]. In addition, the commercially available FEA code ABAQUS was used to model the non-linear piezoelectric effect due to the axial preload applied on the bimorph actuator. The three-dimensional model consisting of two layers of PZT-5A fibers embedded in an epoxy matrix, four Kapton layers, two adhesive layers and an aluminum substrate are shown in figure 7(a). The geometrical data and material properties used in the FEA analysis are shown in table 1. The polarity of the piezoceramic and voltage applied to rectangular fibers are depicted in figure 7(b). The material and geometric properties for critical components of the smart wing design are shown in table 1. The leading edge and composite spar of the smart wing were not modeled since they did not contain any active components. The overall dimensions of the bimorph actuator configuration of the trailing edge with both active and inactive regions were 98 mm × 0.585 mm × 0.765 mm. The bimorph actuator was modeled using approximately 13 000 20-node piezoelectric solid brick elements.

The MFC structure was modeled such that the upper MFC extended while the lower MFC contracted, thus creating a piezoelectric bending actuator. The electric potential for each MFC was set independently to 2000 V as recommended by the MFC manufacturer for the operating voltage range [15]. The skin with latex or the EAP was modeled. The in-house FE solver, however, does not take into account geometric non-linear problems. Therefore, all geometric non-linear analyses

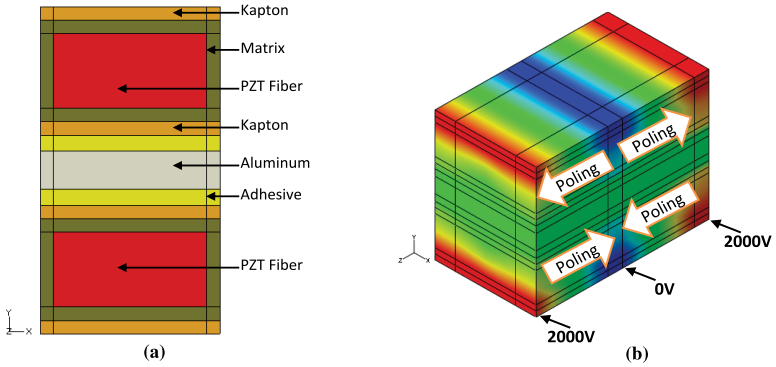

Figure 7. Finite element model (a) geometry and material with (b) voltage and polarization.

Table 5. Comparison of predicted trailing edge tip deflection without EAP skin.

Axial load (N)	Analytical model (deg)	Finite element model (deg)	Difference (%)
0	13.6	12.1	11
15	17.0	13.9	18
35	21.0	16.2	23
40	24.2	18.1	25

were carried out in ABAQUS and all linear analyses were carried out in the in-house FEA code and ABAQUS. For the linear analysis, the results between ABAQUS and the in-house code matched very closely. The results of the FEA analyses for the trailing edge with a latex skin at different incremental axial loads are compared with the analytical predictions in table 5. Compared to the analytical model, the difference in the trailing edge tip deflection predicted by the finite element model varied from 11% to 25% depending on the axial load applied to the bimorph actuator. This difference was attributed to the simplicity of the analytical model which did not account for the reduction in the actuation due to inactive edges, the geometric non-linear condition due to the applied compressive axial load and the coupled electro-mechanical constitutive equations. In contrast, the finite element model accounted for both the active region with piezoceramic material and the inactive region outside the electrode that consisted of passive structural material such as the aluminum substrate, Kapton, and the bonding layer. As expected, 0 N axial loading condition generated the smallest variation between results from the two models because higher axial loads resulted in larger deflections that led to decreases in the accuracy of the analytical model. However, the results showed that the analytical model can be used confidently for parametric studies of the smart wing concept because it provided a good estimate of the resultant deflection as well as correctly predicting the trend in performance. This fact is important because the analytical model required less computational power and significantly less time to generate prediction results compared to the finite element model.

In addition, coupled electro-mechanical constitutive equations in the finite element models were used to predict the effect of aerodynamic loading on the active trailing edge flap. The FEA results confirmed the effect of the aerodynamic loads shown in figure 5, which produce a minor reduction in deflection.

4. Experimental verification

The EA-MAV test article with integrated MFC based bimorph actuators for the trailing edge is shown in figure 8. A center spar fabricated from carbon fiber pre-preg was used to connect the active trailing edge and the leading edge corresponded to the NACA 0009 airfoil profile. Several fabrication techniques were used to verify the bimorph actuator manufacturing as well as the resulting deflection performance. The axial compressive preload on the actuators was introduced using rubber bands during this initial investigation because the skin could not be integrated due to attachment difficulties. Further research is required to develop an attachment mechanism to strain the skin and to provide compliant electrodes to EAP material.

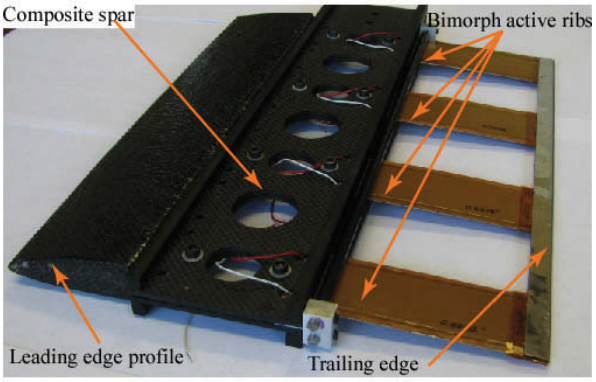

Figure 8. Smart wing hardware model.

Commercially available MFC actuators of type M8528-P1[3] were used to manufacture the bimorph bender actuators for the smart wing hardware. These MFC actuators consisted of an active area of 85 mm × 28 mm. The bending actuators were fabricated by bonding two 0.3 mm thick MFC actuators on either side of a 76 μm aluminum substrate using Loctite E120HP[4] epoxy. The bimorph actuators were cured under pressure for several hours at room temperature prior to testing. A total of four bimorph actuators consisting of MFC were used to assemble the active trailing edge flap. A metal strip connecting the free end of the bimorph actuators was used to form a continuous trailing edge for the smart wing.

Nominal actuator performance tests were conducted to measure the bending deflection of a bimorph actuator. The nominal actuation was defined as the out-of-plane tip deflection where no external loads were applied to the bimorph actuator. This parameter was used as the primary metric to measure the actuation capability of the active flap based on bimorph actuators. The free strain measurement test setup was designed to accurately measure the bending deflection while minimizing undesired external loads, such as frictional loads. The actuator was mounted as a cantilever on a custom fabricated test rig manufactured from Plexiglas for high voltage isolation. For the test, one end of the actuator was clamped to the test rig, while the other end was allowed to deflect freely.

A Keyence LK-086[5] high accuracy laser displacement sensor was used to measure the tip displacement. The laser sensor was installed on the test rig using an X–Y stage in order to focus the laser within the measuring range. A high voltage sinusoidal electrical signal was supplied to the MFCs using two Trek 50/750[6] high voltage amplifiers. The amplifier was configured to supply its maximum $1500V_{pp}$ in the range from 0 to 1500 V. For the experimental investigation, a maximum voltage of $1500V_{pp}$ was applied to the MFC actuators instead

[3] Smart Materials Corp, Sarasota, FL.
[4] Henkel, Düsseldorf, Germany.
[5] Keyence Corporation, Woodcliff Lake, NJ.
[6] Trek Inc., Medina, NY.

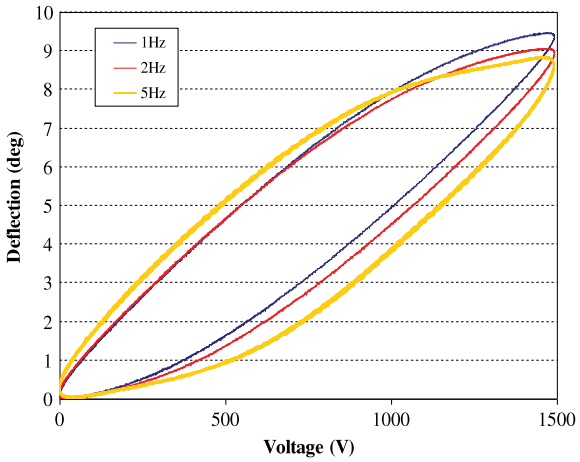

Figure 9. Bimorph actuator hysteresis.

of 2000V_{pp}, as recommended by the manufacturer, due to limitation of the high voltage power amplifier. Two out-of-phase input signals were generated using a MATLAB[7] xPC Target system and fed to the high voltage amplifiers to actuate the opposing MFC actuators in the bimorph. The MATLAB xPC Target was able to generate frequency sweeps as well as sinusoidal signals at specified frequencies while maintaining the phase difference between the two signals. The Nicolet Vision data acquisition system was used to record the bending displacement and the applied voltage simultaneously. The recorded data were exported to Excel for post-processing and additional data analyses. Although bulky high voltage power amplifiers were used for bench testing of this smart wing, lightweight power electronics have been developed by several researchers to integrate piezoceramic actuators in MAV for flight applications [22, 23].

4.1. Effect of voltage

The actuation hysteresis in figure 9 shows a typical deflection of a bimorph actuated at 1, 2, and 5 Hz with a 1500V_{pp} amplitude. This non-linear hysteretic behavior was typically observed in piezoceramic actuators. The highest deflection was measured at 1 Hz with the deflection performance rolling-off with the frequency. Similar behavior was found with bulk PZT-5A piezoceramic [24]. The variations in bending deflection performance of four bimorph actuator specimens along with the averaged deflection at various voltage cycles are shown in table 6. The scatter in the bending performance of bimorph actuators may be attributed to the variations in the manufacturing process and the variation in piezoelectric strain performance in individual MFC actuators. An average deflection of 8.3° for 1500V_{pp} at 1 Hz is in the same order of magnitude as the analytical and finite element modeling results. For an applied voltage of 1500V_{pp}, the analytical and finite element models predicted a deflection of 10.2° and 9.0° that resulted in a difference of 19% and 8%, respectively. This 8% variation in the finite element model prediction with the

[7] The MathWorks Inc., Natick, MA.

Table 6. Bimorph actuator bending performance.

Specimen label	500V_{pp} 1 Hz	1000V_{pp} 1 Hz	1500V_{pp} 1 Hz	1500V_{pp} 2 Hz	1500V_{pp} 5 Hz
MFC14	1.5°	4.4°	7.6°	7.3°	7.1°
MFC24	2.0°	5.5°	8.8°	8.3°	8.0°
MFC26	1.7°	4.5°	7.2°	6.8°	6.6°
MFC28	2.6°	6.1°	9.4°	9.1°	8.8°
Average	1.9°	5.1°	8.3°	7.9°	7.6°

averaged experimentally measured deflection may be attributed to the discrepancies between the actual and published material properties, such as the piezoceramic coupling coefficient, used for the analysis. The larger variation of 19% with the analytical model was caused by the simplifications in the model which did not account for the reduction in the actuation due to inactive regions and other non-linear effects. Although the finite element model accounted for both the inactive and active regions, the analytical model only accounted for the active area of MFC with interdigitated electrode fingers with both polarities in the center of the actuator. It was experimentally determined that a deflection reduction of approximately 6% was caused by the inactive edges in the MFC outside of the electrode. Passive structural material such as the aluminum substrate, Kapton, and bonding layers that existed outside the active area resulted in an inactive region that acted as a constraint to actuation and resulted in a reduction in the measured deflection performance of the bimorph actuator.

4.2. Effect of axial force

The effect of the axial compressive force on the trailing edge deflection was verified by applying calibrated rubber bands and pre-strained latex skin on the bimorph actuators. The compressive axial load on the bimorph actuator generated a geometric non-linear coupling effect on the initial deflection caused by the piezoelectric effect. Application of two rubber bands, four rubber bands, and the pre-stretched latex skin introduced discrete levels of compressive loads on the bimorph actuation, namely 15 N, 30 N, and 40 N, respectively. The roller mechanism designed to apply controlled preload to the skin was not used because it required further improvement before it could be used. The average deflection measured for four samples of bimorph actuators with several levels of axial load is shown in table 7 along with corresponding model predictions and their variations. The trailing edge deflection was increased from 8.3° to 13.6° by using a latex skin that applied approximately 40 N preload to the bimorph actuator. As expected, variations in the deflection predicted by the analytical model were larger than those results from the finite element model. The increase in deflection for the sample MFC28 is shown in figure 10. The results show that the axial compressive preload enhanced the actuation deflection of the piezoceramic bimorph actuator for various applied voltage levels, namely, 500, 1000, and 1500V_{pp}. The non-linear increase in bending deflection due to axial preload and applied voltage was clearly demonstrated by the measured data. Extrapolation of the measured data for 40 N preload to 2000V_{pp} showed that deflection would increase to

Table 7. Comparison of measured tip deflection with predicted results.

Axial load (N)	Measured average (deg)	Analytical model (deg)	Variation with analytical model (%)	Finite element model (deg)	Variation with finite element model (%)
0	8.3	10.2	19	9.0	8
15	9.7	12.6	24	10.5	8
35	12.1	15.6	23	12.3	2
40	13.6	18.0	24	13.9	2

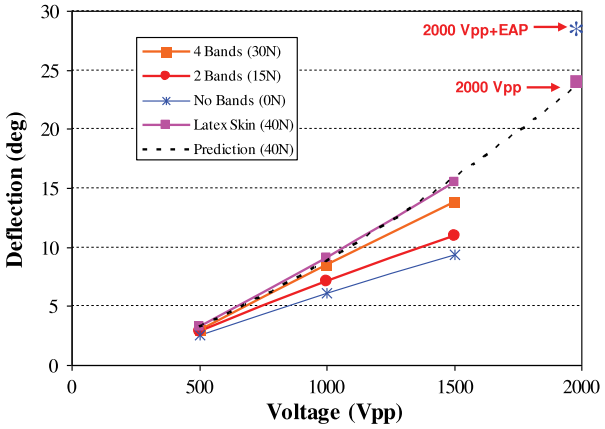

Figure 10. Effect of axial compressive load on MFC28.

22.5° by using the full operating voltage as recommended for the MFC instead of the $1500V_{pp}$, which was limited by the high voltage power amplifier used in the experiment. This predicted deflection was expected to increase further to 27.3° by replacing the passive latex skin with five layers of EAP skin. These results show that the proposed smart wing concept with the dual active material systems could reach a trailing edge bi-directional deflection of approximately 30° required for effective EA-MAV flight control. However, further investigation is required to develop reliable compliant electrodes to integrate the EAP skin to the MAV wing assembly.

To understand the impact of compressive axial load on the dynamic responses of the actuators, a dynamic sweep test was conducted on the same actuator sample. The frequency of the driving voltage was swept from 1 to 50 Hz in 60 s to measure the dynamic response of the bimorph actuator. The data showed that the resonance peak decreased from 40.4 Hz with no rubber bands to 36.3 Hz with two rubber bands and further to 32.6 Hz with four rubber bands. The decrease in the resonance peak indicated that the reduction in effective stiffness of the bimorph actuator structure was due to the applied compressive preload. This behavior was also evident from the analytical model results published previously [14]. The maximum theoretical axial load would be the bucking load of the bimorph and would result in a resonance frequency of zero. This behavior of effective reduction in the bimorph actuator stiffness sets a limit on the compressive axial load applied to the wing. However, it will not adversely affect the operation of the smart wing when the load is properly designed to operate in a quasi-static condition instead of a structural resonance condition.

5. Conclusion

A special class of fixed-wing MAV is currently being designed to fly and hover to provide the range superiority and the hover capabilities to accomplish a variety of surveillance missions. A proposed smart wing concept for EA-MAVs consisting of a dual active material system, namely a piezoceramic fiber actuator as the primary actuation mechanism and EAP as the secondary mechanism to enhance deflection performance has been analyzed and tested. Integration of the two active material systems generated a unique synergetic enhancement of the airfoil trailing edge deflection, as a result of the positive coupling among the piezoelectric effect of the bimorph actuator, the buckling effect on the actuator from the compressive axial load of the pre-strained skin, and the electrostatic effect of the dielectric EAP skin. A simplified analytical model as well as a FEA model were developed to evaluate the trailing edge deflection of the proposed smart wing concept under applicable flight conditions. Furthermore, several bimorph actuators were manufactured to measure quasi-static and dynamic responses of the bimorph actuators. The experimental results validated the analytical and FEA models used to predict the performance of the smart wing design. Experimentally measured data showed that the trailing edge deflection increased from 8.3° to 13.6° for an applied voltage of $1500V_{pp}$ by using a latex skin that applied approximately 40 N preload to the bimorph actuator. This deflection was expected to reach 27.3° by integrating an EAP skin and operating the MFC in a voltage range of $2000V_{pp}$. Experimental results verified the analytical and FEA results that predicted the target bi-directional deflection of approximately 30° could be reached under the proposed flight conditions.

Acknowledgments

The authors would like to thank L Hurtubise, T Kay, and B Lawrie from the Structures and Materials Performance Laboratory of the Institute for Aerospace Research of the National Research Council Canada for providing technical support. In addition, co-op student K Kraemer from the Directorate of Technical Airworthiness and Engineering Support of the Department of National Defence provided invaluable support during the initial design and manufacturing stages of this project.

References

[1] Roskam J 2003 *Airplane Design, Part V: Component Weight Estimation* (Lawrence, KS: Design Analysis & Research Corporation) chapter 7.1

[2] Wickramasinghe V K and Hagood N W 2004 Material characterization of active fiber composites for integral twist-actuated rotor blade application *Smart Mater. Struct.* **13** 1155–65

[3] Bilgen O, Kochersberger K and Inman D J 2008 A novel aerodynamic vectoring control airfoil via macro-fiber-composite actuators? *AIAA 2008-1700, 49th AIAA/ASME/ASCE/AHS/ASC Structures, Structural Dynamics, and Materials Conference (Schaumburg, IL, April 2008)*

[4] Bent A A and Hagood N W 1995 Improved performance in piezoelectric fiber composites using interdigitated electrodes *Smart Structures and Materials Conference*; *Proc. SPIE* **2441** 196–212

[5] Wilbur M L, Mirick P H, Yeager W T Jr, Langston C W, Cesnik C E S and Shin S J 2002 Vibratory loads reduction testing of the NASA/Army/MIT active twist rotor *J. Am. Helicopt. Soc.* **47** 123–33

[6] Wickramasinghe V K, Chen Y and Zimcik D G 2007 Experimental evaluation of a full-scale advanced hybrid buffet suppression system for the F/A-18 vertical tail *J. Aircr.* **44** 733–40

[7] Garcia H, Abdulrahim M and Lind R 2003 Roll control for a micro air vehicle using active wing morphing *AIAA Guidance, Navigation, and Control Conference* (Austin, TX: AIAA) Paper No. AIAA-2003-5347

[8] Barrett R, Vos R, Tiso P and DeBreuker R 2005 Postbuckled precompressed (PBP) actuators: enhancing VTOL autonomous high speed MAVs *46th AIAA/ASME/ASCE/AHS/ASC Structures, Structural Dynamics and Materials Conf.* (Austin, TX: AIAA) Paper No. AIAA-2005-2113

[9] Vos R, Barrett R, de Breuker R and Tiso P 2007 Post-buckled precompressed elements: a new class of control actuators for morphing wings UAVs *Smart Mater. Struct.* **16** 919–26

[10] Wickramasinghe V K and Hagood N W 2004 Durability characterization of active fiber composite actuators for helicopter rotor blade applications *J. Aircr.* **41** 931–7

[11] Melnykowycz M, Kornmann X, Huber C, Barbezat M and Brunner A J 2006 Performance of integrated active fiber composites in fiber reinforced epoxy laminates *Smart Mater. Struct.* **15** 204–12

[12] Wilkie W K, Bryant R G, High J W, Fox R L, Hellbaum R F, Jalink A Jr, Little B D and Mirick P H 2000 Low-cost piezocomposite actuator for structural control applications *SPIE's 7th Annual Int. Symp. on Smart Structures and Materials: Industrial and Commercial Applications of Smart Structures Technologies* vol 399 (Bellingham, WA: The International Society for Optical Engineering) pp 323–34

[13] Park C, Waltz C and Chopra I 1996 Bending and torsion models of beams with induced-strain actuators *Smart Mater. Struct.* **5** 98–113

[14] Wickramasinghe V, Chen Y, Nejad-Ensan M, Martinez M, Wong F and Kraemer K 2008 Verification of a smart wing design for a micro-air-vehicle through simulation *CansSmart: International Workshop on Smart Materials and Structures (Montreal, QC)*

[15] Smart Material Corporation 2008 *The Macro Fiber Composite (MFC)—General Technical Information* www.smart-material.com/Smart-choice.php?from=MFC (cited 19 June)

[16] Morgan Matroc Corporation *Properties of Electro Ceramic Ceramics—Technical Publication TP-226* www.morganelectroceramics.com/pdfs/tp226.pdf cited 9 Sept. 2009

[17] Spadoni A and Ruzzene M 2007 Static aeroelastic response of chiral-core airfoils *J. Intell. Mater. Syst. Struct.* **18** 1067–75

[18] Farhat C and Lesoinne M 2000 Two efficient staggered algorithms for the serial and parallel solution of three-dimensional nonlinear transient aeroelastic problems *Comput. Methods Appl. Mech. Eng.* **182** 499–515

[19] Drela M 2008 XFOIL subsonic airfoil development system http://web.mit.edu/drela/Public/web/xfoil/ (cited 29 July)

[20] Martinez M, Melnykowycz M, Artemev A and Nitzsche F 2005 Finite element analysis of actuated fiber composites *CansSmart: International Workshop on Smart Materials and Structures (Toronto, ON)*

[21] Martinez M, Chen Y, Wickramasinghe V, Wong F and Kraemer K 2008 Adaptive airfoil wing for micro UAV flight control *ICAST 2008: Proc. 19th Int. Conf. Adaptive Structures and Technologies (Ascona)*

[22] Bilgen O, Kochersberger K, Diggs E C, Kurdila A J and Inman D J 2007 Morphing wing micro-air-vehicles via macro-fiber-composite actuators *Proc. 48th AIAA/ASME/ASCE/AHS/ASC Structures, Structural Dynamics, and Materials Conference (Honolulu, April 2007)* AIAA-2007-1785

[23] Vos R, de Breuker R, Barrett R and Tiso P 2007 Morphing wing flight control via postbuckled precompressed piezoelectric actuators *J. Aircr.* **44** 1060–8

[24] Jaffe B, Cook W R and Jaffe H 1971 *Piezoelectric Ceramics* (New York: Academic)